Controlled Potential Electrolysis: Transition from Fast to Slow Regimes in Homogeneous Molecular Catalysis. Application to the Electroreduction of CO2 Catalyzed by Iron Porphyrin

Rana Deeba, Alexandra Collard, Camille Rollin, Florian Molton, Sylvie Chardon-noblat, Cyrille Costentin

ChemElectroChem

Research Article
doi.org/10.1002/celc.202300350

Chemistry Europe
European Chemical Societies Publishing

www.chemelectrochem.org

VIP *Very Important Paper*

Special Collection

Controlled Potential Electrolysis: Transition from Fast to Slow Regimes in Homogeneous Molecular Catalysis. Application to the Electroreduction of CO_2 Catalyzed by Iron Porphyrin

Rana Deeba,[a] Alexandra Collard,[a] Camille Rollin,[a] Florian Molton,[a] Sylvie Chardon-Noblat,[a] and Cyrille Costentin*[a]

Dedicated to Prof. Flavio Maran for his 70th birthday

Molecular catalysis of electrochemical reactions is a field of intense activity because of the current interest in electrifying chemical transformations, including both electrosynthesis of organic molecules and production of fuels via small molecule activation. Controlled potential electrolysis (CPE) is often coupled with *in situ in operando* spectroscopic methods with the aim to gather mechanistic information regarding the catalytic species involved. Herein, considering a simple mechanism for a homogeneous molecular catalysis of an electrochemical reaction, we establish the concentration profile of the catalyst in the electrolysis cell enabling to envision the information that can be obtained from the coupling of this CPE with a spectroscopic probe in the cell compartment. We show how the characteristic parameters of the system (catalytic rate constant, cell dimensions and stirring rate) affect the response with particular emphasis on the transition between two limiting cases, namely a 'fast' catalysis regime where catalysis only takes place in a small layer adjacent to the electrode surface and a 'slow' catalysis regime where catalysis takes place in the bulk of the solution. These formal concepts are then illustrated with an experimental example, the electroreduction of CO_2 in dimethylformamide homogeneously catalyzed by iron tetraphenylporphyrin and followed by UV-vis spectroscopy.

Introduction

Molecular catalysis of electrochemical reactions is a field of intense activity because of the current interest in electrifying chemical transformations, including both electrosynthesis of organic molecules[1] and production of fuels via small molecule activation.[2–5] Rational design of molecular catalysts for a given reaction implies to decipher the mechanism,[6] including degradation pathways.[7] Non-destructive analytical techniques such as cyclic voltammetry (CV) are very useful for mechanistic analysis.[8] However, controlled potential electrolysis (CPE) is often required for product identification and quantification as well as for catalyst durability evaluation.[9] To that end, CPE can be coupled with *in situ* / *in operando* spectroscopic methods, entering here the realm of spectroelectrochemistry (SEC). The goal might be to identify the product formed during electrolysis or/and to follow the time evolution of the various catalyst forms with the aim to detect intermediates or transformation or degradation of the catalyst. SEC has thus been used as a tool to investigate molecular catalytic processes for a long time[10] and many developments have been made[11] including recent ones regarding the use of XAS spectroscopy.[12] Even considering only CPE, the outcome of a SEC experience is sensitive to the experimental conditions for molecular catalysis in solution due to inherent inhomogeneous concentrations in an electrolysis cell. Despite several formal descriptions of SEC experiments for molecular catalytic systems considering various configurations (light beam normal or parallel to the electrode surface; thin-layer or larger cells) being available,[13] reports on experimental SEC do not always pay attention to it in the data analysis and interpretation. Herein, we propose a simple modelling of CPE for a homogeneous catalytic reaction in a three electrode electrochemical cell configuration corresponding to typical laboratory-scale experiments as sketched in scheme 1. The main purpose is to establish the concentrations profiles in the cell enabling to envision the information that can be obtained from the coupling of this CPE with spectra recorded with a spectroscopic probe. Importantly, we wish to establish how the characteristic parameters of the system (catalytic rate constant, cell dimensions and stirring rate) affect the response with particular emphasis on the transition between two limiting cases, namely a 'fast' catalysis regime where catalysis only takes place in a small layer adjacent to the electrode surface and a

[a] R. Deeba, A. Collard, C. Rollin, F. Molton, Dr. S. Chardon-Noblat, Prof. Dr. C. Costentin
Univ Grenoble Alpes, CNRS, DCM, 38000 Grenoble, France
E-mail: cyrille.costentin@univ-grenoble-alpes.fr

Supporting information for this article is available on the WWW under https://doi.org/10.1002/celc.202300350

Special Collection An invited contribution to the Flavio Maran Festschrift

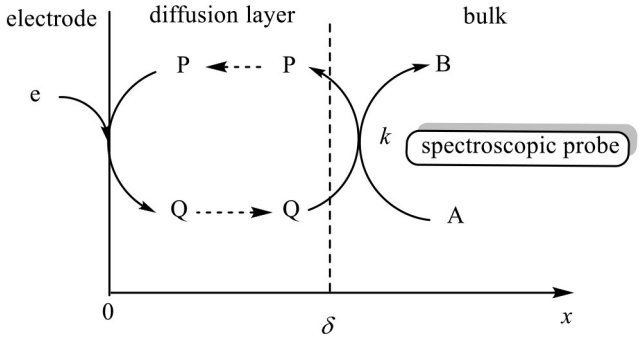

Scheme 1. Schematic view of the CPE of a homogeneous catalytic reaction with a spectroscopic probe in the electrochemical cell bulk solution. x is the distance from the electrode and δ is the size of the diffusion layer.

'slow' catalysis regime where catalysis takes place in the bulk of the solution.

For the sake of simplicity, we restrict our approach to an ideal catalytic system as depicted in scheme 1 in which the catalytic reaction is a simple one-electron/one-step process with a fast P/Q redox couple (the catalyst). Q reacts with a substrate A in solution yielding the product B and regenerating P with a rate constant k. The system is ideal in the sense that there is no degradation of P or Q over the course of the electrolysis and only one product is formed. We first analyze the case of CPE with a constant concentration of substrate. Then, we discuss the situation of consumption of the substrate, hence exhaustive controlled potential electrolysis. In both cases, we will focus our attention on the evolution of the catalytic species concentration in the bulk of the solution. The concepts formalized in this study are finally illustrated with an experimental example, namely the electroreduction reaction of CO_2 (CO_2ERR) in dimethylformamide (DMF) homogeneously catalyzed by iron tetraphenylporphyrin (FeTPP) and followed by in situ UV-vis spectroscopy.

Results and Discussion

Cyclic Voltammetry

As a preliminary to our discussion, we first recall the cyclic voltammetry (CV) response of the system considered in scheme 1. With excess of substrate, the CV response is given by the following analytical expression (equation 1):[14]

$$\frac{1}{\sqrt{\pi}}\int_{-\infty}^{\xi}\frac{\psi\exp[-\lambda_{CV}(\xi-\eta)]}{\sqrt{\xi-\eta}}d\eta=\frac{1}{1+\exp(-\xi)} \quad (1)$$

with the dimensionless current and potential being respectively $\psi=\frac{i}{FSC_P^0\sqrt{DFv/RT}}$ and $\xi=F\left(E_{P/Q}^0-E\right)/RT$. Importantly, the CV response is governed by a single dimensionless parameter $\lambda_{CV}=\frac{kC_A^0}{Fv/RT}$ measuring the ratio of the timescale of the CV and the timescale of the homogeneous reaction. As illustrated in Figure 1, for small values of λ_{CV}, the CV trace corresponds to a simple reversible nernstian wave indicating that no catalysis takes place in the timescale of the CV. In other words, CV is not a useful technique to investigate slow catalytic processes, keeping in mind that scan rates smaller than 20 mV/s should be avoided to prevent interference of natural convection perturbing the semi-infinite planar diffusion regime. As λ_{CV} is increased the CV loses its reversibility and reaches a canonical S-shape at large value of λ_{CV} (Figure 1). This last behavior corresponds to pure-kinetics conditions resulting from a mutual compensation of diffusion of Q and its reaction with A so that the catalytic reaction only takes place within a thin diffusion-reaction layer close to the electrode surface. The CV plateau current is thus given by $i_{pl}=FSC_P^0\sqrt{DkC_A^0}$ giving a direct access to the evaluation of the rate constant, hence showing that CV is a convenient technique to investigate fast catalytic processes.

Controlled Potential Electrolysis

We now consider controlled potential electrolysis. We assume that the diffusion is linear and can be treated in the context of the Nernst layer approximation. The size of the diffusion layer, δ, is set by the values of the diffusion coefficient (assumed to be identical for all species), the kinematic viscosity and the rate of stirring or circulation of the solution.[15] As shown in the supporting information (SI), the system is governed by two dimensionless parameters, $\lambda_{el}=\frac{kC_P^0}{D/\delta^2}$ and $p=\frac{V/S}{\delta}$, together with the excess factor $\gamma=\frac{C_A^0}{C_P^0}$. λ_{el} measures the competition between the catalytic reaction and diffusion within the diffusion layer and p is the ratio between the 'length' of the electrochemical cell and the size of the diffusion layer. We first make the simplifying assumption that the concentration of the substrate A is uniform both in the bulk and in the diffusion layer and remains constant throughout the electrolysis. Such a situation

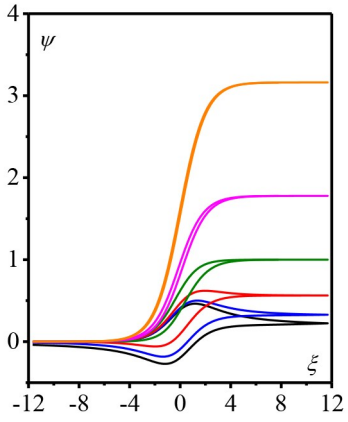

Figure 1. Dimensionless CV responses for a one electron/one-step catalytic reaction with excess of substrate as function of the dimensionless parameter λ_{CV}. $\log\lambda_{CV}$ =-1.5 (black), −1 (blue), −0.5 (red), 0 (green), 0.5 (magenta), 1 (orange). Adapted with permission from Ref. [8].

can be observed when the substrate is in large excess or when its concentration is maintained constant. Moreover, we consider that the constant applied potential E is negative enough compared to the standard potential $E^0_{P/Q}$ so that the concentration of P at the electrode surface is zero. It is thus shown (see SI) that the concentration of Q in the bulk of the solution is given by equation 2:

$$\frac{[Q]_{bulk}}{C_P^0} = \frac{1}{\cosh\left(\sqrt{\lambda_{el}\gamma}\right)} \frac{1-\exp\left[-\left(p\lambda_{el}\gamma + \frac{\sqrt{\lambda_{el}\gamma}}{\tanh\left(\sqrt{\lambda_{el}\gamma}\right)}\right)\frac{t}{t_{cell}}\right]}{p\sqrt{\lambda_{el}\gamma}\tanh\left(\sqrt{\lambda_{el}\gamma}\right)+1} \quad (2)$$

with $t_{cell} = V\delta/DS$ and the concentration of Q in the diffusion layer is (equation 3):

$$\frac{[Q]}{C_P^0} = \cosh\left(\frac{x\sqrt{\lambda_{el}\gamma}}{\delta}\right) + \left(\frac{\frac{[Q]_{bulk}}{C_P^0} - \cosh\left(\sqrt{\lambda_{el}\gamma}\right)}{\sinh\left(\sqrt{\lambda_{el}\gamma}\right)}\right)\sinh\left(\frac{x\sqrt{\lambda_{el}\gamma}}{\delta}\right) \quad (3)$$

where x is the distance from the electrode surface and $0 < x < \delta$. There is an initial transient regime corresponding to accumulation of Q with a characteristic time t_{acc} (equation 4):

$$t_{acc} = t_{cell}/\left(p\lambda_{el}\gamma + \frac{\sqrt{\lambda_{el}\gamma}}{\tanh\left(\sqrt{\lambda_{el}\gamma}\right)}\right) \quad (4)$$

After this transient regime, a steady-state catalytic regime is obtained, with (equation 5):

$$\frac{[Q]_{bulk,ss}}{C_P^0} = \frac{1}{\cosh\left(\sqrt{\lambda_{el}\gamma}\right)} \times \frac{1}{p\sqrt{\lambda_{el}\gamma}\tanh\left(\sqrt{\lambda_{el}\gamma}\right)+1} \quad (5)$$

and the corresponding catalytic current is (equation 6):

$$\frac{i_{cat}}{FSC_P^0\sqrt{DkC_A^0}} = \frac{\cosh\left(\sqrt{\lambda_{el}\gamma}\right) - \frac{1}{\cosh\left(\sqrt{\lambda_{el}\gamma}\right)} \times \frac{1}{p\sqrt{\lambda_{el}\gamma}\tanh\left(\sqrt{\lambda_{el}\gamma}\right)+1}}{\sinh\left(\sqrt{\lambda_{el}\gamma}\right)} \quad (6)$$

From these general expressions, several limiting cases can be delineated. First, we note that $p < 1$ corresponds to a thin layer electrolysis cell, i.e., $l = V/S$ very small, leading to $\frac{i_{cat}}{FSC_P^0\sqrt{DkC_A^0}} = \tanh\left(\sqrt{\lambda_{el}\gamma}\right)$ and $\frac{[Q]}{C_P^0} = \frac{\cosh\left[(1-y)\sqrt{\lambda_{el}\gamma}\right]}{\cosh\left(\sqrt{\lambda_{el}\gamma}\right)}$. Therefore, two limiting behaviors are obtained in the context of thin layer constant potential electrolysis. 'Fast' steady-state catalysis occurs when $\lambda_{el}\gamma \gg 1$ (FTL zone). The catalytic process takes place in a very small layer adjacent to the electrode surface which thickness is $\sqrt{D/kC_A^0}$ and only a small fraction f_Q of catalyst is under the form of Q, $f_Q = 1/\sqrt{\lambda_{el}\gamma} \to 0$. P is therefore the resting state of the catalyst. Alternatively, 'slow' steady-state catalysis occurs when $\lambda_{el}\gamma \ll 1$ (STL zone). The catalytic process occurs in the whole thin-layer electrolysis cell and $\frac{i_{cat}}{FV} = kC_P^0C_A^0$. The resting state of the catalyst is Q because $f_Q = \tanh\left(\sqrt{\lambda_{el}\gamma}\right)/\sqrt{\lambda_{el}\gamma} \to 1$. This analysis shows that a spectroelectrochemistry experiment in a thin layer cell with a light beam probing the whole cell length cannot provide information on Q in the 'fast' catalytic regime.

We now consider the situation of $p > 1$. Again, we can distinguish a 'fast" catalytic regime and a 'slow" catalytic regime. 'Fast' catalysis regime still corresponds to $\lambda_{el}\gamma \gg 1$ with catalysis taking place in a thin layer within the diffusion layer (FK zone). Therefore $\frac{i_{cat}}{FSC_P^0\sqrt{DkC_A^0}} = 1$ and $[Q]_{bulk,ss} \to 0$, i.e. nothing happens in the bulk of the reaction. Note that $t_{acc} \ll t_{cell}$, indicating that the steady state regime is reached very quickly. A 'slow' catalysis regime is obtained when $\lambda_{el}\gamma \ll 1$. However, in this regime, two limiting cases can be encountered depending on value of the parameter. $\kappa_{el}\gamma\kappa_{el}\gamma = \lambda_{el}\gamma \times p = \frac{kC_A^0}{DS/V\delta}$. $\kappa_{el}\gamma$ compares the kinetics of the catalytic reaction to the characteristics time of the electrochemical cell t_{cell}. If $\kappa_{el}\gamma < 1$ (SK zone), then $\frac{i_{cat}}{FV} = kC_A^0C_P^0$ and $[Q]_{bulk,ss} \approx C_P^0$. Catalysis is so slow that all catalyst molecules are transformed into Q in the solution during the transient period and, then, Q reacts with A which is converted into B while the regenerated P is converted back to Q via a back-and-forth transport to the electrode surface that is fast on the timescale of the chemical transformation. Considering $\kappa_{el}\gamma > 1$ (DK zone), we obtain $i_{cat} = \frac{FSDC_P^0}{\delta}$ and $\frac{[Q]_{bulk,ss}}{C_P^0} = \frac{1}{\kappa_{el}\gamma} \to 0$. Catalysis takes place only in the bulk of the solution but it is limited by the diffusion of the electrogenerated Q across the diffusion layer. All regimes are conveniently summarized in a two-dimensional zone diagram shown in Figure 2. The corresponding expressions of the catalytic current and Q steady-state concentration in the bulk are gathered in Table 1. The compass rose in Figure 2 indicates how the variation of the parameters (rate constant k, cell characteristics V and S, substrate concentration C_A^0 and size of the diffusion layer δ) moves the system in the diagram.

Figure 3a represents the evolution of the concentration profile of Q as function of the parameter $\lambda_{el}\gamma$ (for example via variation of the concentration of the substrate C_A^0) for a large value of p (here, $p = 100$), a usual situation in laboratory scale electrolysis. Starting with a large value of $\lambda_{el}\gamma$ corresponding to

Table 1. Characteristics of limiting behaviors.

Limiting behavior	i_{cat}	$[Q]_{bulk,ss}$
FK	$FSC_P^0\sqrt{DkC_A^0}$	0
SK	$FVkC_P^0C_A^0$	C_P^0
DK	$\frac{FSDC_P^0}{\delta}$	$\frac{C_P^0}{\kappa_{el}\gamma}$
SLT	$FVkC_P^0C_A^0$	C_P^0
FLT	$FSC_P^0\sqrt{DkC_A^0}$	0

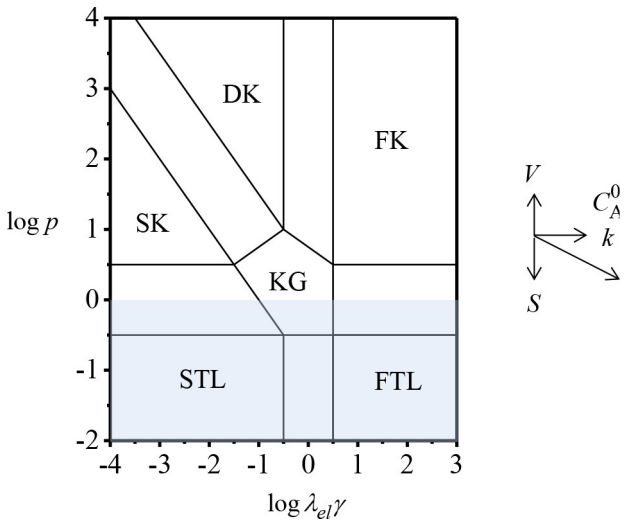

Figure 2. Schematic zone diagram for CPE as a function of the two dimensionless parameters $p = \frac{V/S}{\delta}$ and $\lambda_{el}\gamma = \frac{kC_A^0}{D/\delta^2}$. KG: general case (equations (5) and (6)). SK: slow catalysis. FK: fast catalysis. DK: diffusion case. The light blue region corresponds to thin layer. STL: thin layer slow catalysis. FTL: thin layer fast catalysis. The arrows summarize how the variations of the parameters move the system from one zone to the other. Zones without names are transition zones.

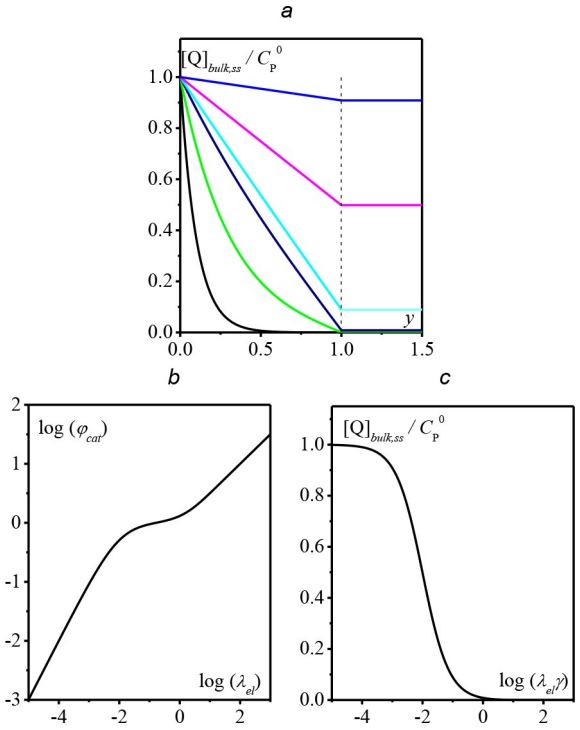

Figure 3. (a) Concentration profiles of Q as function of $\lambda_{el}\gamma$ for $p = 100$. $\log(\lambda_{el}\gamma)$ =-3 (blue), −2 (magenta), −1 (cyan), 0 (navy), 1 (green), 2 (black). (b) $\varphi_{cat} = \frac{i_{cat}}{FSC_P^0 D/\delta}$ as function of $\lambda_{el}\gamma$ for $p = 100$. (c) $\frac{[Q]_{bulk,ss}}{C_P^0}$ as function of $\lambda_{el}\gamma$ for $p = 100$.

the 'fast' catalysis regime, Q is indeed squeezed in a thin reaction layer in the diffusion layer. As $\lambda_{el}\gamma$ is decreasing, the size of reaction layer increases and hits the size of the diffusion layer. The corresponding evolution of the catalytic current and of the concentration of Q in the bulk solution are shown in Figures 3b and 3c respectively. The dimensionless current $\varphi_{cat} = \frac{i_{cat}}{FSC_P^0 D/\delta}$ decreased when $\lambda_{el}\gamma$ is decreasing because kC_A^0 is decreasing but with a 0.5 slope in logarithm scale due to the simultaneous increase of the reaction layer size with is inversely proportional to $\sqrt{kC_A^0}$. Then $\varphi_{cat} = \frac{i_{cat}}{FSC_P^0 D/\delta}$ reaches a plateau equal to 1. The catalytic reaction is now extended to the whole solution because the active form of the catalyst starts to accumulate in the bulk of the solution and triggers transformation of A to B in a larger volume. However, the process is limited by the diffusion of Q across the diffusion layer. When $\lambda_{el}\gamma$ is further decreased, i.e., a decrease of the catalysis kinetics compared to the diffusion kinetics, $\varphi_{cat} = \frac{i_{cat}}{FSC_P^0 D/\delta}$ decreased because the catalytic reaction becomes so slow that replenishment of Q in the solution is no more limiting. In this 'slow' regime eventually obtained, the electrolysis cell behaves as a homogeneous reactor in which the reductant Q is constantly provided and the volumic rate is $\frac{i_{cat}}{FV} = kC_A^0 C_P^0$.

As expected, for 'fast' catalysis, the concentration of Q in the bulk is nil (Figure 3c). Probing the bulk solution with a spectroscopic technique cannot be informative on the catalytic process, the thin diffusion-reaction layer being difficult to be specifically probed. As the system transitions toward 'slow' catalysis, Q starts to accumulate in the bulk and becomes the dominant resting state when the 'slow' catalysis regime is reached. Probing the bulk solution with a spectroscopic technique can then provide information on the resting state species.

Exhaustive Potentiostatic Electrolysis

We now consider a more complicated situation where the substrate A is consumed during the electrolysis. As shown in the SI, the concentration of A in the bulk of the solution is given by (equation 7):

$$\frac{[A]_{bulk}}{C_P^0} = \gamma + \frac{[Q]_{bulk}}{C_P^0} - \int_0^\tau \frac{i_{cat}}{FSDC_P^0/\delta} d\tau \qquad (7)$$

with $\tau = \frac{t}{t_{cell}}$. To make the analysis tractable, we assume that the concentration of A is uniform within the bulk and the diffusion layer, meaning that the diffusion of A is fast and/or that catalysis is not too fast. We also restrict our analysis to the steady-state regime assuming that the initial concentration of A is large enough for remaining constant during the initial transient regime which is then identical to the one described above. Numerical calculation of combined equations (5), (6) and (7) with γ replaced by $\frac{[A]_{bulk}}{C_P^0}$ in equations (5) and (6) allows getting the time evolution of $[A]_{bulk}$, $[Q]_{bulk}$ and $\frac{i_{cat}}{FSDC_P^0/\delta}$ as function of the dimensionless parameters $\lambda_{el} = \frac{kC_P^0}{D/\delta^2}$, $p = \frac{V/S}{\delta}$ as well as γ. A typical example is shown in Figure 4, considering again a large value of p ($p = 100$), a usual situation in laboratory scale

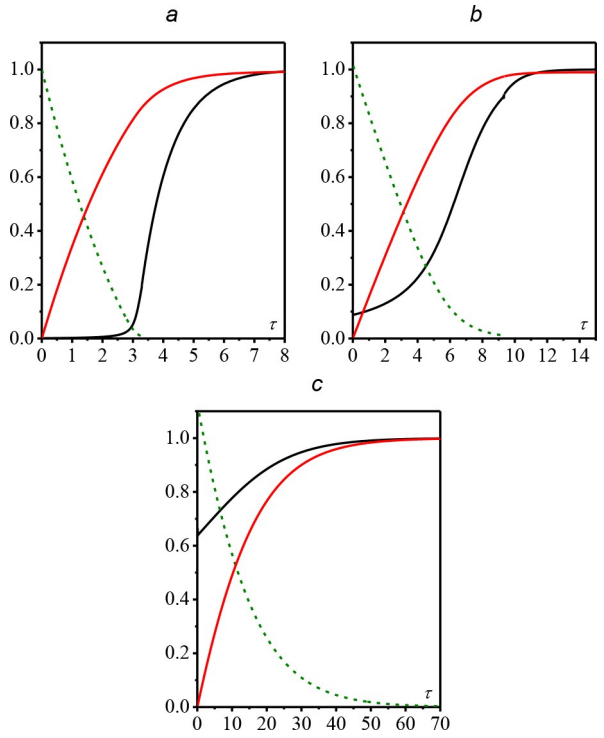

Figure 4. Exhaustive controlled potential electrolysis. Evolution as function of the dimensionless time $\tau = t/t_{cell}$ of the dimensionless steady-state bulk concentration of Q ($\frac{[Q]_{bulk,ss}}{C_P^0}$ in black), the relative dimensionless passed charge (Q/Q_{max} in red) and the dimensionless substrate concentration ($\frac{[A]_{bulk,ss}}{C_P^0}$ in dashed green) with: $p = 100$, $\gamma = 5$ and $\log \lambda_{el}$ =0 (a), −1.7 (b) and −3 (c).

electrolysis. To evaluate the effect of A consumption, we take $\gamma = 5$ so that exhaustive potentiostatic electrolysis corresponds to the transfer of a dimensionless charge $Q_{max} = \int_0^\infty \varphi_{cat} d\tau = \gamma + 1 = 6$. Figure 4a represents the case of $\lambda_{el}\gamma = 5$, hence a 'fast' catalysis situation when electrolysis starts. The system remains in the 'fast' catalysis regime until complete consumption of A because it is seen that the concentration of Q in the bulk is negligible. At the end of electrolysis, Q builds up in the bulk. An intermediate situation is represented in Figure 4b. The steady state concentration of Q in the bulk at the beginning of the electrolysis is small but slightly increases as electrolysis progresses and slows down because A is consumed. At the end of electrolysis, 90% of the catalyst is under the form of Q in the bulk. This example illustrates the transition of the system from 'fast' to 'slow' catalysis during electrolysis due to the substrate consumption progressively slowing down catalysis. Finally, the situation shown in Figure 4c exemplifies an almost fully 'slow' catalysis regime. Q is already the dominant catalyst species in the bulk after the transient regime. Its concentration increases as catalysis progresses and reaches its maximal value $[Q]_{bulk,ss} = C_P^0$ before the end of the exhaustive catalysis.

Application to CO_2 CPE Catalyzed by FeTPP

Efficient electrochemical conversion of CO_2 to any reaction product (carbon monoxide, formic acid, formaldehyde, methanol, methane…) requires catalytic schemes. A large number of molecular catalysts for the homogeneous electrochemical CO_2 conversion have been proposed.[4] They mainly derive from transition metal complexes by electrochemical generation of an appropriately reduced state, which is restored by the catalytic reaction scheme. Iron porphyrins are one of the most studied families of such catalysts. It has indeed been shown more than three decades ago that reduction of iron(III) tetraphenylporphyrin (Fe(III)TPP) in organic solvent by three electrons (formally to Fe(0)TPP[16]) allows reduction of CO_2 to CO.[17] Since then, many studies regarding the mechanism of this reaction have been reported, with particular emphasize on the effect of co-substrates such as Lewis acids[18] or proton donors on the catalytic activity,[19] as well as the effect of substituents on the porphyrin moiety.[20–24] The large variation of the apparent catalytic rate constant upon addition of co-substrates offers the opportunity to tune the catalytic regime. Moreover, noting that the UV-vis signature of the various redox states of FeTPP are well-characterized,[25] this system appears as a suitable platform to illustrate the CPE concepts described in the present study using UV-vis *in operando* spectroelectrochemistry within a lab electrolysis cell. Note that the goal here is not to establish the already known mechanism[18–20] but to illustrate the concepts described above. The typical set-up used for electrolysis is described in the SI. The working electrode is a vitreous carbon felt electrode. The volume of the catholyte is 10 mL for experiments run under argon and 18 mL for experiments run under a flux of CO_2. The CV of Fe(III)TPPCl in DMF under argon exhibits three reversible waves (Figure 5a). Successive exhaustive electrolysis under argon at –0.92, −1.42 and –1.87 V vs. SCE with in situ UV-vis analysis of the electrolyte solution allows to identity the intermediates Fe(II)TPP, Fe(I)TPP and Fe(0)TPP via their Q-band signatures in agreement with literature data (Figure 5b and SI for additional details). Each electrolysis corresponds to the passage of 1 electron per FeTPP as exemplified in Figures 5c and 5d for the Fe(III)TPP/Fe(II)TPP conversion. From the charge vs. time variation which closely matches the Fe(III)TPP to Fe(II)TPP conversion followed at 690 nm, the time constant of the cell is evaluated as $t_{cell} = \frac{V\delta}{DS_{elec}}$ =100 s (Figure 5d), with a stirring rate of 900 rpm. We note that, although the UV-vis spectra obtained at the end of the second electrolysis has features corresponding to Fe(I)TPP, the band at 615 nm is shifted to the expected value at 605 nm (Figure S3a and Table S1). [25,26] An EPR spectrum of the solution obtained after electrolysis was recorded at 100 K (Figure S4). It shows the characteristic features of Fe(I)TPP ($g_\perp$ =2.3 and $g_\parallel$ =1.93). Another feature, corresponding to one asymmetric line characterizing an anisotropic $g_\perp$ =1.95, is observed and attributed to a mixed valence Fe(III)-Fe(III) μ-oxo-bis(FeTPP) dimer.[27,28] Finally, a contribution from an organic radical ($g = 2$) attributed to free porphyrin is also seen. Simulation of the EPR spectrum indicates that the solution contains 95% Fe(I)TPP, 4.7% of mixed valence Fe(II)-Fe(III) μ-oxo-bis(FeTPP) dimer and

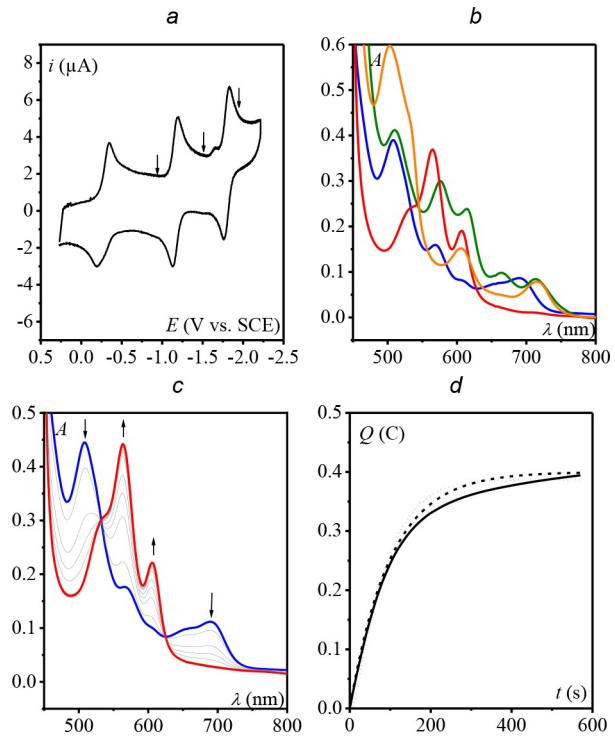

Figure 5. (a) FeTPPCl 0.4 mM in DMF + 0.1 M NBu_4PF_6 under argon: CV at 0.1 V/s on a 3 mm diameter glassy carbon electrode. (b) UV-vis spectra (Q-bands, l = 1 mm) initial (blue) and after application of constant potential –0.92 (red), −1.42 (green) and –1.87 (orange) V vs. SCE. (c) Time evolution of UV-vis spectra during application of a constant potential −0.92 V vs. SCE; the initial spectrum is in blue and the final spectrum is in red. (d) Time evolution of the charge passed during application of a constant potential −0.92 V vs. SCE. Dashed line: fitting with $Q = Q_{max}[1 - \exp(-t/t_{ell})]$. Dotted line: time evolution of the normalized absorbance at 690 nm according to: $Q_{max}\left[1 - \left(A_{690} - A_{690,t=\infty}\right)/\left(A_{690,t=0} - A_{690,t=\infty}\right)\right]$.

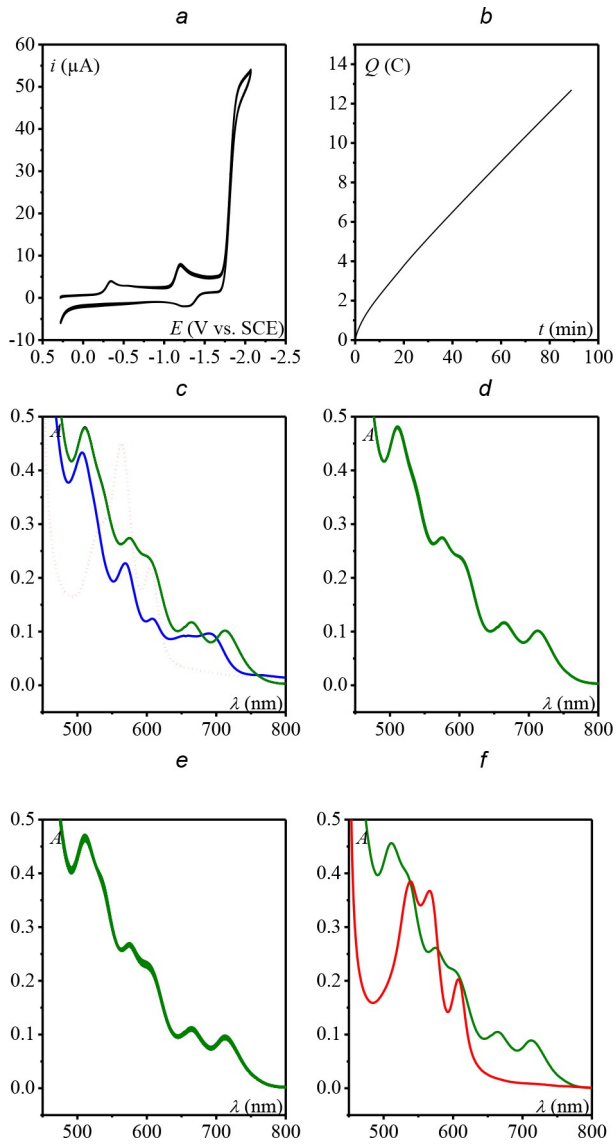

Figure 6. FeTPPCl 0.4 mM in DMF + 0.1 M NBu_4PF_6 at 0.1 V/s on a 3 mm diameter glassy carbon electrode under CO_2 and with 6.7 mM of PhOH: (a) CV; (b) Time evolution of the charge passed during application of a constant potential −1.82 V vs. SCE (18 mL solution); (c) UV-vis spectra (Q-bands, l = 1 mm) during application of a constant potential −1.82 V vs. SCE. Blue: initial spectrum, dotted red: spectrum after 3 min, green: spectrum after 30 min. (d) Overlay of UV-vis spectra during application of a constant potential −1.82 V vs. SCE between t = 20 min to t = 90 min (one spectrum / 10 s). (e) Overlay of UV-vis spectra during application of a constant potential −1.52 V vs. SCE (one spectrum / 10 s) after 90 min electrolysis at −1.82 V vs. SCE. (f) UV-vis spectra before (green) and after (red) application of a constant potential at −0.72 V to the solution obtained after (e).

0.3% of free porphyrin (Figure S4). The observation of a mixed valence Fe(II)-Fe(III) μ-oxo-bis(FeTPP) dimer is in agreement with the report that Fe(III)-Fe(III) μ-oxo-bis(FeTPP) dimer monoelectronic reduction occurs at the same potential as Fe(II)TPP reduction to Fe(I)TPP.[26] Further reduction of this mixed valence dimer at slightly more negative potential leads to breaking of the μ-oxo-dimer and formation of Fe(I)TPP (Figure S5).

Under an atmosphere of CO_2 (0.23 M)[29] and in the presence of 6.7 mM of phenol as a source of protons, the CV exhibits at large S-shaped catalytic wave with a half-wave potential $E_{1/2}$ equal to the standard potential of the Fe(I)TPP/Fe(0)TPP couple $E^0_{Fe(I)TPP/Fe(0)TPP}$ (Figure 6a). This criterion matches with the proposed simplified mechanism[30] shown in Scheme 2.

In this framework, the catalytic rate constant can be evaluated from the plateau current i_{pl} using $i_{pl}/i_p^0 = 2.24\sqrt{2k_{cat}RT/Fv}$ where i_p^0 is the peak current corresponding to the catalyst under argon. We obtain k_{cat} = 86 s^{-1}. Electrolysis was then run at constant potential −1.82 V vs. SCE corresponding approximately to the half-wave potential of the Fe(I)TPP/Fe(0)TPP couple. In the first minutes of electrolysis, the species in the bulk is converted from Fe(III)TPP to Fe(II)TPP and then to Fe(I)TPP (Figure 6c). While the applied potential corresponds to a mixture of both Fe(I)TPP and Fe(0)TPP as thermodynamically stable species based on the Nernst equa-

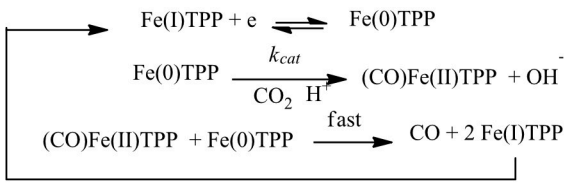

Scheme 2. Reaction scheme for CO_2 electroreduction catalyzed by FeTPP.

tion, no Fe(0)TPP is seen as the two bands at 664 and 714 nm have similar intensities whereas Fe(0)TPP would only exhibit a band at 714 nm (Figure 6d). It is in line with the observation of a linear increase of the passed charge over time (Figure 6b) indicating a sustained catalysis. The resting state in the bulk solution is Fe(I)TPP (Figure 6d) corresponding to a fast catalysis regime. Thus, the steady-state catalytic current is $i_{cat}/2 = FS_{elec}C^0_{cat}\sqrt{2k_{cat}D}/2$ =2.1 mA because the applied potential corresponds to $E_{1/2} = E^0_{Fe(I)TPP/Fe(0)TPP}$, with C^0_{cat} = 0.3 mM and S_{elec} the surface area of the electrolysis working electrode. Taking the plateau current of the CV, $i_{pl} = FS_{CV}C^0_{cat}\sqrt{2k_{cat}D}$ = 52 µA with S_{CV} = 0.07 cm^2 the surface area of the CV working electrode, we obtain S_{elec} =5.65 cm^2. Then, from $t_{cell} = \frac{V\delta}{DS_{elec}}$ =100 s evaluated with V = 10 cm^3 and taking D = 5 10^{-6} cm^2/s, we estimate the size of the diffusion layer set by the stirring as δ =9 µm. Hence, the competition parameters are calculated as $p = \frac{V_{elec}/S_{elec}}{\delta}$ =3.5 10^3 ⩾1 with V_{elec} = 18 cm^3 and $\lambda_{el}\gamma = \frac{2k_{cat}}{D/\delta^2}$ =27.5 ⩾1 in agreement with a system been in a fast catalysis regime. The electrolysis was stopped after 90 min and the potential was then switched to −1.52 V vs. SCE. At this potential, the catalytic current is residual and the UV-vis indicates that the catalytic species in solution is still Fe(I)TPP (Figure 6e) with no degradation. Switching then the potential to −0.72 V vs. SCE, the Fe(I)TPP is converted to a mixture of Fe(II)TPP and (CO)Fe(II)TPP (Figure 6f). The presence of Q-bands characteristic of (CO)Fe(II)TPP as identified from an authentic sample (see SI), confirms that the product formed upon electrolysis is CO as previously shown by thin layer spectroelectrochemistry.[31] Because of the small solubility of CO in DMF, the stirring of the solution and the constant flux of CO_2 through the cell, only a fraction of Fe(II)TPP has a coordinated CO hence leading to the observed mixture. No degradation of the catalyst had occurred during electrolysis as attested both by CV (Figure S8) and absence of decrease of the UV-vis intensity of the resting state Fe(I)TPP (Figure 6d). The fraction of catalyst actually involved in the electrolysis can be evaluated from the ratio of the length of the diffusion reaction layer $\sqrt{D/2k_{cat}}$ = 2.4 10^{-4} cm and the length of the cell V_{elec}/S_{elec} =3.185 cm. Only 0.0076% of the catalyst molecules present in solution are actually active, i.e. under the form of Fe(0)TPP during steady-state catalysis.

Still in the presence of FeTPP as catalyst, electrolysis was performed with a smaller concentration of CO_2 and no addition of phenol so as to get a slower catalytic process. A 10 mL solution of 0.4 mM of FeTPPCl was thus first electrolyzed under argon at −1.42 V generating a solution of Fe(I)TPP (Figure 7a). Then, while keeping the applied potential at −1.42 V, 1.2 mL of a solution previously saturated with CO_2 was added corresponding to a concentration of 25 mM of CO_2 in the electrolysis cell and the potential was switched to −1.82 V thus triggering catalysis. In the bulk of the solution, while catalysis was running, the UV-vis spectrum evolution indicates a conversion of Fe(I)TPP to Fe(0)TPP (Figure 7b). However, the conversion of Fe(I)TPP to Fe(0)TPP monitored by the absorbance at 665 nm (Figure 7c) does not follow the same pace as the charge accumulation (Figure 7d). This situation is typical of a system transitioning from 'fast' catalysis to 'slow' catalysis due to the decrease of the

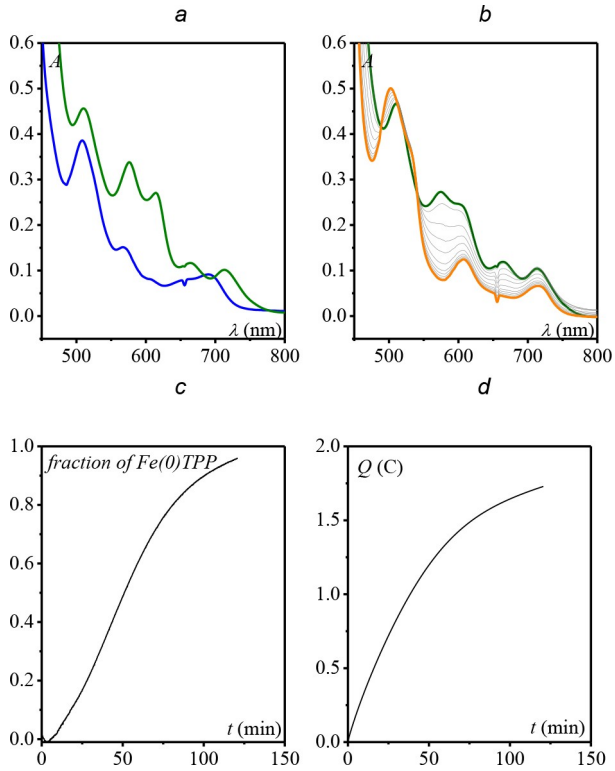

Figure 7. FeTPPCl 0.4 mM in DMF + 0.1 M NBu_4PF_6 under argon: (a) UV-vis spectra (Q-bands, l = 1 mm) before (blue) and after application of constant potential –1.42 V vs. SCE (green). (b) Time evolution of UV-vis spectra in the presence of CO_2 (25 mM) during application of a constant potential −1.82 V vs. SCE; the initial spectrum is in green and the final spectrum is in orange (one scan / 13 min). (c) Fraction of Fe(0)TPP in the bulk of the solution during application of a constant potential −1.82 V vs. SCE to a 11.2 mL solution of 0.4 mM Fe(I)TPP (prepared in (b)) in DMF + 0.1 M NBu_4PF_6 with 30 mM of CO_2. The fraction is obtained from the absorbance at 665 nm in (b): $\left[1 - \left(A_{665} - A_{665,t=\infty}\right)/\left(A_{665,t=0} - A_{666,t=\infty}\right)\right]$. (d) Time evolution of the charge passed during application of a constant potential −1.82 V vs. SCE to a 11.2 mL solution of 0.4 mM Fe(I)TPP (prepared in (b)) in DMF + 0.1 M NBu_4PF_6 with 25 mM of CO_2.

apparent rate constant because of consumption of the substrate (see Figure 4b). In the present case, we surmise that consumption of the proton source (presumably residual H_2O from the solvent and supporting electrolyte) is responsible for this transition rather than consumption of CO_2 which is in large excess (25 mM).

These results confirm that Fe(I)TPP is the resting state in the CO_2 to CO electroreduction catalyzed by FeTPP in our electrolysis cell. The active form of the catalyst seems to be Fe(0)TPP. Recently, it was reported that the triply reduced Fe(III)TPP, formally Fe(0)TPP, forms an adduct with CO_2 and that this adduct is the active form of the catalyst.[32] Intriguingly, the UV-vis spectrum recorded under CO_2 at a potential corresponding to catalysis (−1.72 V vs. SCE) and attributed to this adduct has the same features as the doubly reduced Fe(III)TPP, i.e. formally Fe(I)TPP. In light of the present analysis, we alternatively propose that the detected species, both in UV-vis and XAS, is actually Fe(I)TPP. Indeed, based on the catalytic current in CV shown in that paper, the rate constant can be evaluated as $2k_{cat}$ ≈4 s^{-1} leading to a diffusion-reaction layer length of

11 μm whereas the length of the cell is 200 μm making the active form of the catalyst at steady-state only ca. 6% of the catalyst with the doubly reduced Fe(III)TPP, i.e. Fe(I)TPP or an adduct between Fe(I)TPP and CO_2, being the dominant resting state (94%).

Conclusions

We have investigated the behavior of a simple molecular catalytic system of an electrochemical reaction in controlled potential electrolysis. We have shown how the characteristic parameters of the system (catalytic rate constant, cell dimensions and stirring rate) affect the response, i.e., catalytic current at steady-state in conditions of excess of substrate. Two limiting regimes can be obtained: a 'fast' catalysis regime where catalysis only takes place in a small layer adjacent to the electrode surface and a 'slow' catalysis regime where catalysis takes place in the bulk of the solution. In the transition between these regimes, the catalytic current may be controlled by the diffusion of the catalyst across the diffusion layer. In exhaustive electrolysis conditions, i.e., when the substrate is consumed during electrolysis, a transition between fast and slow catalysis regime can be observed over the course of the electrolysis and diagnosed from the mismatch on the time evolution of the passed charge and the evolution of the species of the catalyst present in the bulk solution monitored by spectroscopic method. Application of these concepts to the electroreduction of CO_2 to CO in DMF catalyzed by FeTPP indicates that the resting state in the solution is Fe(I)TPP, as supported by both UV-vis and EPR spectroscopies, provided that a proton donor is present to sustain fast catalysis.

Experimental Section

Cyclic voltammograms (CV) were obtained by use of CHI 750E potentiostat equipped with a standard three-electrode cell. The working electrode was a commercial 3 mm-diameter glassy carbon (GC) disk. The counter-electrode was a platinum wire and the reference electrode was Ag/Ag^+ ($AgNO_3$ 10 mM) electrode in acetonitrile + 0.1 M NBu_4PF_6 in acetonitrile.

Electrolysis were performed using a Solartron Analytical Instrument potentiostat (Modulab XM MTS) using XM-studio software. All experiments were performed under argon or CO_2 with a carbon felt working electrode attached to a glassy carbon rod. The reference electrode was an Ag/Ag^+ ($AgNO_3$ 10 mM) in acetonitrile + 0.1 M NBu_4PF_6 with an acetonitrile + 0.1 M NBu_4PF_6 electrolyte bridge and the counter electrode a platinum wire in a bridge separated from the electrolytic cell by a glass frit. *In-situ/in operando* UV-vis spectra were recorded with an UV-vis quartz probe (l = 1 mm) immersed in electrolyte cell, on a MCS 501 UV-Vis-NIR (Carl Zeiss) diode array spectrophotometer equipped with an automatic shutter.

EPR samples were taken under inert atmosphere and placed directly into liquid nitrogen until analysis. X-band EPR spectra were recorded at 100 K with a EMX Plus Bruker spectrometer equipped with a ER4119HS Bruker cavity.

Supporting Information

Derivation of the equations. Numerical calculations. Additional experimental details. Additional references[33–38].

Acknowledgements

The MITI (Mission pour les Initiatives Transverses et Interdisciplinaires) program of the CNRS is gratefully acknowledged for RD doctoral financial support. This work was partially supported by the Agence Nationale de la Recherche: Labex ARCANE, CBH-EUR-GS, ANR-17-EURE-0003 and ANR-22-CE07-0028-01. The Initiatives de Recherche à Grenoble Alpes (IRGA program) is acknowledged for financial support. The NanoBio ICMG (UAR 2607), is acknowledged for providing facilities for EPR analyses.

Conflict of Interests

The authors declare no conflict of interest.

Data Availability Statement

The data that support the findings of this study are available from the corresponding author upon reasonable request.

Keywords: Electrolysis · Catalysis · Spectroelectrochemistry · CO_2 reduction · Iron Porphyrin

[1] a) M. Yan, Y. Kawamata, P. S. Baran, *Chem. Rev.* **2017**, *117*, 13230–13319; b) E. Steckhan, *Angew. Chem. Int. Ed.* **1986**, *25*, 683; c) C. Costentin, J-M. Savéant, *Proc. Natl. Acad. Sci. USA.* **2019**, *116*, 11147.
[2] J. R. McKone, S. C. Marinescu, B. S. Brunschwig, J. R. Winkler, H. B. Gray, *Chem. Sci.* **2014**, *5*, 865.
[3] M. L. Pegis, C. F. Wise, D. J. Martin, J. M. Mayer, *Chem. Rev.* **2018**, *118*, 2340.
[4] E. Boutin, L. Merakeb, B. Ma, B. Boudy, M. Wang, J. Bonin, E. Anxolabéhère-Mallart, M. Robert, *Chem. Soc. Rev.* **2020**, *49*, 5772.
[5] S. J. K. Forrest, B. Schluschas, E. Y. Yuzik-Klimova, S. Schneider, *Chem. Rev.* **2021**, *121*, 6522–6587.
[6] C. Costentin, J–M. Savéant, *Nat. Chem. Rev.* **2017**, *1*, 0087.
[7] K. J. Lee, B. D. McCarthy, J. L. Dempsey, *Chem. Soc. Rev.* **2019**, *48*, 2927.
[8] J–M. Savéant, C. Costentin, Elements of Molecular and Biomolecular Electrochemistry. Wiley 2nd Ed. 2019.
[9] C. Costentin, G. Passard, J–M. Savéant, *J. Am. Chem. Soc.* **2015**, *137*, 5461.
[10] J. W. Strojek, T. Kuwana, *J. Electroanal. Chem.* **1968**, *16*, 471.
[11] J. J. A. Lozeman, P. Führer, W. Olthuis, M. Odjik, *Analyst* **2020**, *145*, 2482.
[12] D. Mendoza, S.-T. Dong, B. Lassalle-Kaiser, *Curr. Opin. Colloid Interface Sci.* **2022**, *61*, 101635.
[13] a) E. Laborda, J. M. Gomez-Gil, A. Molina, R. G. Compton, *Electrochim. Acta* **2018**, *284*, 721; b) Y. Xie, S. Dong, *J. Electroanal. Chem.* **1990**, *291*, 1; c) S. Dong, Y. Xie, *J. Electroanal. Chem.* **1992**, *335*, 197; d) N. Winograd, H. N. Blount, T. Kuwana, *J. Phys. Chem.* **1969**, *73*, 3456.
[14] J.-M. Savéant, E. Vianello, *Recherches sur les courants catalytiques en polarographie oscillographique à balayage linéaire de tension. Étude théorique. In Advances in Polarography*, 1 ed., Longmuir, I. S., Ed., Pergamon Press: Cambridge, U.K., **1959**, Vol. 1, pp 367–374.
[15] K. V. Shanthanam, A. Bard (Ed.), *J. Electroanalytical Chemistry*, vol. 4, Marcel Dekker, New York, pp. 212–315.
[16] a) It has been reported[16b] that Fe(I)TPP and Fe(0)TPP in THF are best described by $Fe(II)TPP^{\bullet-}$ and $Fe(II)TPP^{\bullet\bullet 2-}$. For the sake of simplicity we

use the formal oxidation state Fe(I)TPP and Fe(0)TPP; b) C. Romelt, J. Song, M. Tarrogo, J. A. Rees, M. van Gastel, T. Weyhehermuller, S. DeBeer, E. Bill, F. Neese, *Inorg. Chem.* **2017**. *56*, 4746.
[17] M. Hammouche, D. Lexa, J-M. Savéant, M. Momenteau, *J. Electroanal. Chem.* **1988**. *249*, 347.
[18] a) M. Hammouche, D. Lexa, J-M. Savéant, M. Momenteau, *J. Am. Chem. Soc.* **1991**, *113*, 8455; b) I. Bhugun, D. Lexa, J–M. Savéant, *J. Phys. Chem.* **1996**, *100*, 19981.
[19] a) I. Bhugun, D. Lexa, J–M. Savéant, *J. Am. Chem. Soc.* **1996**, *118*, 1769; b) C. Costentin, S. Drouet, G. Passard, M. Robert, J–M. Savéant, *J. Am. Chem. Soc.* **2013**, *135*, 9023.
[20] a) I. Azcarate, C. Costentin, M. Robert, J–M. Savéant, *J. Am. Chem. Soc.* **2016**, *138*, 16639; b) I. Azcarate, C. Costentin, M. Robert, J–M. Savéant, *J. Phys. Chem. C* **2016**, *120*, 28951; c) D. J. Martin, J. M. Mayer, *J. Am. Chem. Soc.* **2021**, *143*, 11423.
[21] a) P. Gotico, B. Boitrel, R. Guillot, M. Sircoglou, A. Quaranta, Z. Halime, W. Leibl, A. Aukauloo, *Angew. Chem. Int. Ed.* **2019**, *58*, 4504; b) P. Gotico, L. Roupnel, R. Guillot, M. Sircoglou, W. Leibl, Z. Halime, A. Aukauloo, *Angew. Chem. Int. Ed.* **2020**, *59*, 22451; c) A. Khadhraoui, P. Gotico, W. Leibl, Z. Halime, A. Aukauloo, *ChemSusChem* **2021**, *14*, 1308.
[22] a) E. M. Nichols, J. S. Derrick, S. K. Nistanaki, P. T. Smith, C. J. Chang, *Chem. Sci.* **2018**, *9*, 2952; b) J. S. Derrick, M. Loipersberger, S. K. Nistanaki, A. V. Rothweiler, M. Head-Gordon, E. M. Nichols, C. J. Chang, *J. Am. Chem. Soc.* **2022**, *144*, 11656.
[23] a) C. G. Margarit, N. G. Asimow, M. I. Gonzalez, D. G. Nocera, *J. Phys. Chem. Lett.* **2020**, *11*, 1890; b) C. G. Margarit, C. Schnedermann, N. G. Asimow, D. G. Nocera, *Organometallics* **2019**, *38*, 1219.
[24] S. Sen, B. Mondal, D. Saha, A. Rana, A. Dey, *Dalton Trans.* **2019**, *48*, 5965.
[25] E. Anxolabéhère, G. Chottard, D. Lexa, *New J. Chem.* **1994**, *18*, 889.
[26] R. J. Donohoe, M. Atamian, D. F. Bocian, *J. Am. Chem. Soc.* **1987**, *109*, 5593.
[27] I. A. Cohen, D. Ostfeld, B. Lichtenstein, *J. Am. Chem. Soc.* **1972**, *94*, 4522.
[28] K. M. Kadish, G. Larson, D. Lexa, M. Momenteau, *J. Am. Chem. Soc.* **1975**, *97*, 282.
[29] I. Bhugun, D. Lexa, J–M. Savéant, *Anal. Chem.* **1994**, *66*, 3994.
[30] C. Costentin, J–M. Savéant, *ACS Catal.* **2018**, *8*, 5286.
[31] M. Hammouche, D. Lexa, M. Momenteau, J–M. Savéant, *J. Am. Chem. Soc.* **1991**, *113*, 8455.
[32] D. Mendoza, S–T. Dong, N. Kostopoulos, V. Pinty, O. Rivada-Wheelaghan, E. Anxolabéhère-Mallart, M. Robert, B. Lassalle-Kaiser, *ChemCatChem* **2023**, *15*, e202201298.
[33] EasySpin, *J. Magn. Reson.* **2006**, *178*, 42.
[34] F. Molton, *Magn. Reson. Chem.* **2020**, *58*, 718.
[35] D. Lexa, M. Momenteau, J. Mispelter, *Biochim. Biophys. Acta* **1974**, *338*, 151.
[36] R. J. Donohoe, M. Atamian, D. F. Bocian, *J. Am. Chem. Soc.* **1987**, *109*, 5593.
[37] I. A. Cohen, D. Ostfeld, B. Lichtenstein, *J. Am. Chem. Soc.* **1972**, *94*, 4522.
[38] K. M. Kadish, G. Larson, D. Lexa, M. Momenteau, *J. Am. Chem. Soc.* **1975**, *97*, 282.

Manuscript received: July 21, 2023
Revised manuscript received: August 21, 2023
Version of record online: September 7, 2023